Supplementary Information

Table of Content

1. Additional details about the experimental facility

The quartz jet-stirred reactor has been associated through a molecular-beam sampling system to reflectron time-of-flight mass spectrometer (RTOF MS) combined with tunable synchrotron vacuum ultraviolet photoionization. The experiments were performed at the National Synchrotron Radiation Laboratory (NSRL) in Hefei, China. This part describes in more detail the tunable synchrotron vacuum ultraviolet beamline, the jet-stirred reactor and the molecular-beam sampling and photoionization mass spectrometry.

1.1 The tunable synchrotron vacuum ultraviolet light source

Synchrotron radiation from an undulator of the 800 MeV electron storage ring was monochromized with a 1 m Seya-Namioka monochromator equipped with one laminar grating (1500 grooves/mm, Horiba Jobin Yvon, France). The wavelength of the monochromator was calibrated with the known ionisation energies (IEs) of the inert gases. The beamline provided the photon energy covering from 7.8 to 24 eV with the energy resolving power ($E/\Delta E$) of around 1,000 and the average photon flux of ~10^{13} photons/sec. A gas filter was used to eliminate the higher-order harmonic radiation with Ne or Ar filled in the gas cell. The photon flux was monitored by a silicon photodiode (SXUV-100, International Radiation Detectors, Inc., USA) for normalizing ion signal.

1.2 The jet-stirred reactor

This type of reactor was already used for numerous gas-phase kinetic studies (e.g. [1][2][3]). Figure S1 shows the reactor before the insertion of the sampling cone-like nozzle. It is a spherical reactor in which diluted reactant enters through an injection cross located in its centre. The diameter of the reactor (made in France, Dijonverre Labo) is about 50 mm and its volume is about 90 cm^3. It can be considered as well stirred for a mean residence time (τ) between 0.5 and 6 s (in the latter case, the Reynolds number is 1070 and the recirculation ratio 127)[4]. The stirring of the whole reactor volume is achieved by the mean of four turbulent gas jets directed in different directions and produced by the four nozzles of the injection cross in the centre of the reactor. Inside diameter of the nozzles is about 0.3 mm.

The quartz reactor is preceded by a quartz annular preheating zone in which the temperature of the gases is increased up to the reactor temperature before entering inside. The annular preheater is made of two concentric tubes, the inter-annular distance of which is about 0.5 mm. Gas mixture residence time inside the annular preheater is very short compared to its

residence time inside the reactor (about a few percents). Both spherical reactor and annular preheating zone are heated by the mean of “Thermocoax” heating resistances rolled up around their wall. Reaction temperature measurement is made by means of a thermocouple K (provided by Thermocoax, no correction needed) which is located inside the intra-annular space of the preheating zone and the extremity of which is on the level of the injection cross. The dilution was large enough so that a maximum increase of temperature of 5 K was obtained when starting the reactive gases feeding [5]. The temperatures were controlled by a multi channel regulator (HORST GmbH, Germany). The ratio of inert gas was set slightly below the ratio in air to obtain the largest amounts of products minimizing the occurrence of strong thermal phenomena.

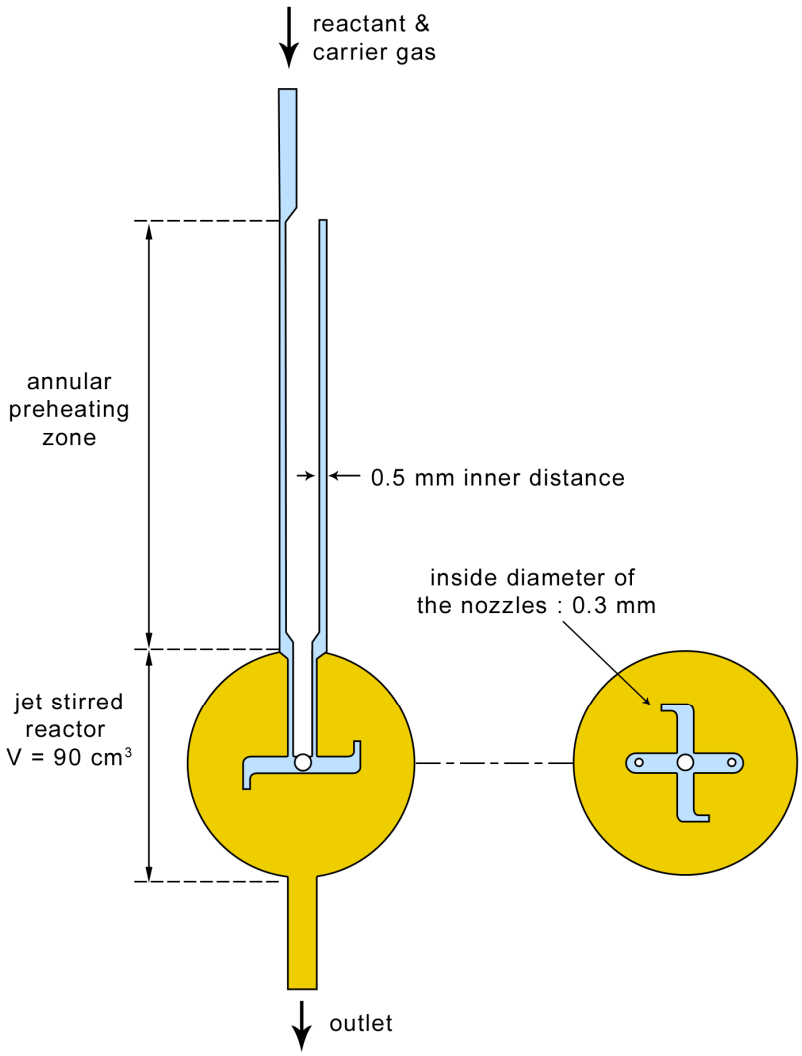

Figure S1. Scheme of the jet-stirred reactor before the insertion of the coupling cone.

The gases used in this study were provided by Dalian Guangming Special Gas Products Co., Ltd., Dalian, China with a purity of +99%. Gas flows were controlled by MKS mass flow controller.

1.3 The molecular-beam sampling and photoionization mass spectrometer

A schematic diagram of the experimental instrument is shown in Figure S2. Briefly, the instrument consists of the jet-stirred reactor, a differentially pumped chamber (**I**) with molecular-beam sampling system, and a photoionization chamber (**II**) with a homemade RTOF MS (China) for ion detection. The coupling with the reactor has been made through a quartz cone-like nozzle with a height of 50 mm and an open angle of 60°. The tip of the cone was pierced with a 75 μm orifice made using sandstone paper before the tip of cone was inserted inside the sphere of the reactor. Figure S3 presents a view of the reactor (covered by the heating resistances) with the tip of the cone inserted inside the quartz sphere and connected to the chamber of the mass spectrometer by a flange made on its other side. The view also presents the nickel skimmer. During the experiments, the reactor and the cone were completely covered by quartz wool.

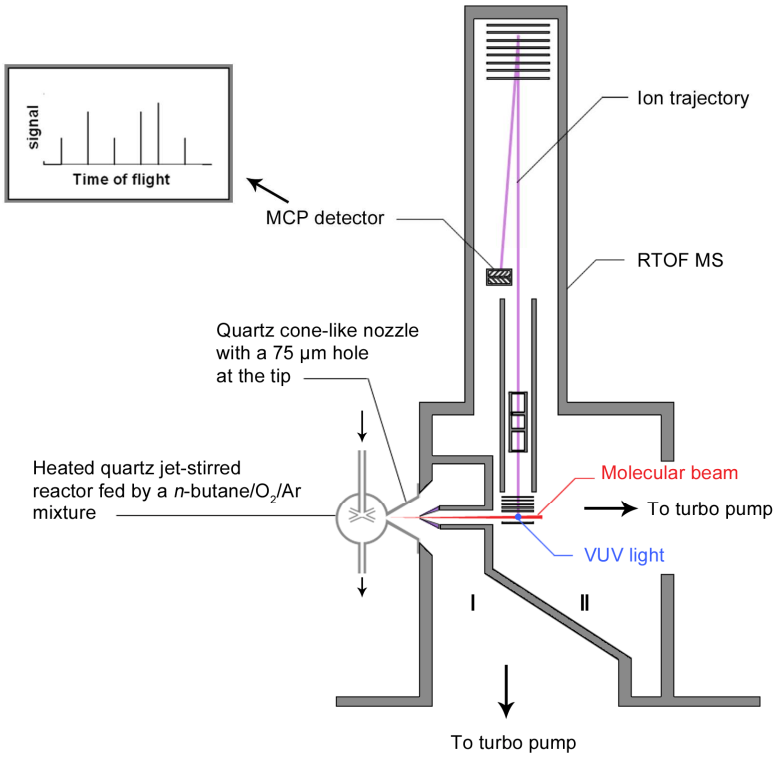

Figure S2. Schematic diagram of the instrument including the heated quartz jet-stirred reactor, the differential pumped chamber (**I**) with molecular-beam sampling system, and the photoionization chamber with the reflectron time-of-flight mass spectrometer (RTOF MS) (**II**).

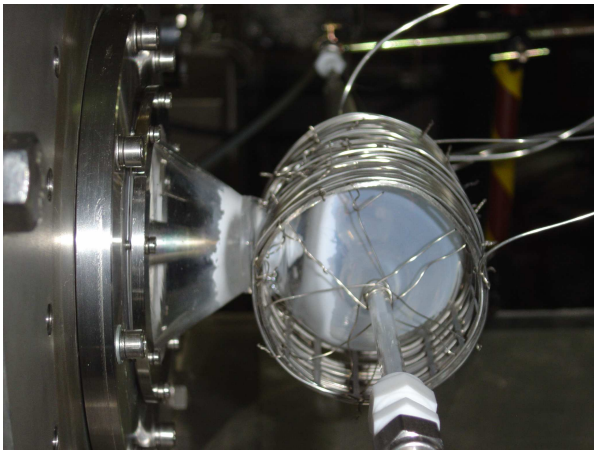

Figure S3. Photography of the reactor with a part of the heating resistances and connected to the differential pumped chamber.

The species from the reactor were sampled through the quartz cone-like nozzle. A nickel skimmer with a 1.25 mm diameter aperture was located 15 mm downstream from the sampling nozzle. The sampled gases formed a molecular beam, which was passed horizontally through the 10 mm gap between the repeller and extractor plates of RTOF MS. The molecular beam intersected perpendicularly with synchrotron vacuum ultraviolet light beam. The differentially pumping chamber (**I**) was pumped with a 1500 l/sec turbomolecular pump, which was backed by a 15 l/sec mechanical pump plus a 70 l/sec roots pump. The photoionization chamber (**II**) and time-of-flight tube were pumped with a 600 and 300 l/sec turbomolecular pumps, respectively, and both with a 15 l/sec mechanical pump. The pressures in the reactor, the differentially pumped chamber and the ionization chamber were 106.4×10^{3}, 6.7×10^{-2}, and 8.3×10^{-4} Pa, respectively.

1.4 The ion detection and data acquisition

The ion signal was detected with a RTOF MS, which was installed in the photoionization chamber vertically (Figure S2). A pulsed voltage of 346 V was used to propel ions into the flight tube, and finally to a multichannel plate (MCP) detector. The total length of the ion flight is 1.8 m. The ion signals were amplified by a pre-amplifier (VT120C, EG&G ORTEC, USA). The mass resolution ($m/\Delta m$) was measured to be ~2000. A digital delay generator (DG535, Stanford Research System, USA) was used to trigger the pulse power supply and to feed as the start of a multiscaler with repetition ratio of 18,000 Hz. The multiscaler (FAST Comtec P7888, Germany) was used to record signals of mass spectrum with 2 ns bin width. A small bias voltage (1.0 V) was added to improve signal intensity, reduce the background ions, and enhance the mass resolution. The relation between the ion signal and the concentration of

a given species has been described in detail by Li et al.[6]. As a first approximation, the normalized ion signal of a given species can often be considered as proportional to its concentration with a factor depending mainly on its photoionization cross section.

2. Experimental ionisation energies of masses 48, 62, 90 and 104

With variation of photon energy, a series of mass spectra are measured, e.g. at a specific temperature, where most oxidation intermediates have high concentrations. The integrated ion signals of each mass peak weighted by photon flux are plotted versus the photon energy, yielding a photoionization efficiency (PIE) spectrum containing precise information of the ionization energies (the initial deflection from the background signal on the PIE spectrum). Because of the cooling effect in molecular beam sampling [7], the discrepancies of measured ionization thresholds caused by the hot band are typically less than 30 meV [8]. Knowing the molecular weight and ionization thresholds can identify the dominant intermediates through the accordance of ionization thresholds and obtained literature IEs, e.g. from NIST online database [9] and many previous calculations. For the candidates of intermediates with unknown IEs, high-level ab initio theoretical methods can be used for IE prediction, especially for the free radicals whose IEs are difficult to be experimentally determined.

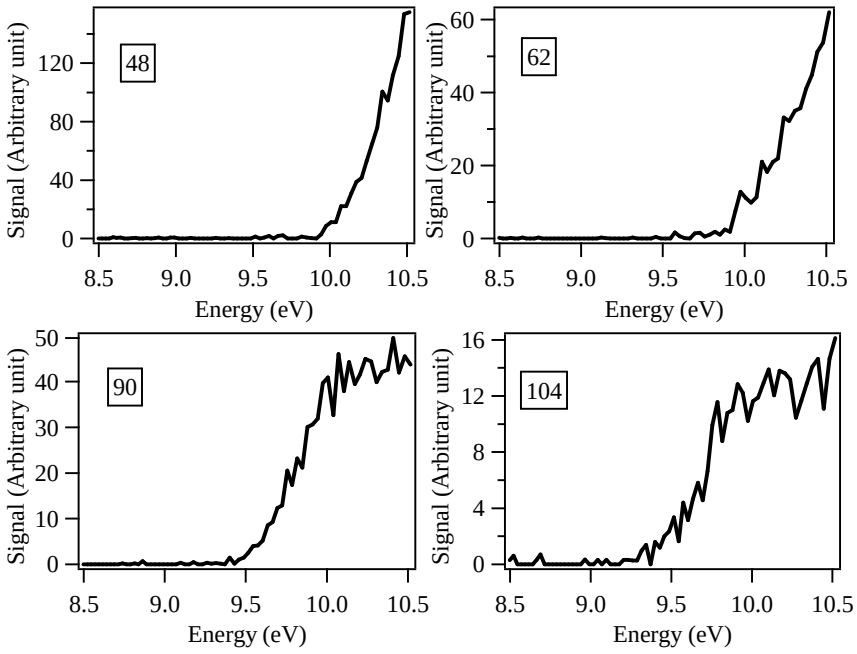

Figure S4: Photoionization efficiency spectra of masses 48, 62, 90 and 104 sampled from the reactor. The temperature in the reactor was 630 K.

Figure S4 presents the experimental signal variations with the photon energy obtained for masses 48, 62, 90, and 104. It shows that the experimental ionization energies are of 9.91, 9.69, 9.37 and 9.29 ± 0.05 eV for masses 48, 62, 90 and 104, respectively.

3. Description of the model used for simulations

The simulations were performed using the software PSR of CHEMKIN [10]. The mechanism of the low-temperature oxidation of n-butane (available on request) has been automatically generated using EXGAS software. This software has already been used for generating mechanisms in the case of a wide range of alkanes [11][12] and alkenes [13]. The reaction mechanisms generated by EXGAS are made of three parts:

- A comprehensive primary mechanism, where the only molecular reactants considered are the initial organic compounds and oxygen. According to the reaction scheme of the oxidation of alkanes described in the main text of this paper, the reactant and the primary radicals are systematically submitted to different types of following elementary steps :
  - Unimolecular initiations involving the breaking of a C-C bond.
  - Bimolecular initiations with oxygen to produce alkyl and $\bullet HO_2$ radicals.
  - Oxidations of alkyl radicals with O_2 to form alkenes and $\bullet HO_2$ radicals.
  - Additions of alkyl (R•) and hydroperoxyalkyl (•QOOH) radicals to an oxygen molecule.
  - Isomerizations of alkyl and peroxy radicals (ROO• and •OOQOOH) involving a cyclic transition state for •OOQOOH radicals.
  - Decompositions of radicals by β-scission involving the breaking of C-C or C-O bonds for all types of radicals (for low temperature modelling, the breaking of C-H bonds is neglected).
  - Decompositions of hydroperoxyalkyl radicals to form cyclic ethers and •OH radicals.
  - Metatheses involving H-abstractions by radicals from the initial reactants.
  - Recombinations of radicals.
  - Disproportionations of peroxyalkyl radicals with $\bullet HO_2$ to produce alkylhydroperoxides and O_2 (disproprtionnations between two peroxyalkyl radicals or beween peroxyalkyl and alkyl radicals are not taken into account).
- A C_0-C_2 reaction base, including all the reactions involving radicals or molecules containing less than three carbon atoms. The fact that no generic rule can be derived for

the generation of the reactions involving every compounds containing less than three atoms of carbon makes the use of this reaction base necessary.

- A lumped secondary mechanism, containing the reactions consuming the molecular stable products of the primary mechanism, which do not react in the reaction base. For reducing the number of reactants in the secondary mechanism, the molecules formed in the primary mechanism, with the same molecular formula and the same functional groups, are lumped into one unique species, without distinguishing between the different isomers. The writing of the secondary reaction is made in order to promote the formation of C_{2+} alkyl radicals, the reactions of which are already included in the primary mechanism [12].

Thermochemical data for molecules or radicals were automatically calculated and stored as 14 polynomial coefficients, according to the CHEMKIN II formalism [10]. These data were automatically calculated using software THERGAS [14], based on the group and bond additivity methods proposed by Benson [15].

The kinetic data of isomerisations, recombinations and the unimolecular decompositions are automatically calculated based on the thermochemical kinetics methods [15] using the transition state theory or the modified collision theory. The kinetic data, for which the calculation is not possible by KINGAS [12], are estimated from correlations, which are based on quantitative structure-reactivity relationships and obtained from a literature review [11].

4. Supplementary References

[1] R. Bounaceur, I. Da Costa, R. Fournet, F. Billaud, F. Battin-Leclerc, *Int. J. Chem. Kin.* **2005**, 37, 25-19.

[2] J. Biet, M.H. Hakka, V. Warth, P.A. Glaude, F. Battin-Leclerc, *Energy and Fuel* **2008**, 22, 2258-2269.

[3] M.H. Hakka, P.A. Glaude, O. Herbinet, F. Battin-Leclerc, *Combust. Flame* 2009, 156, 2129-2144.

[4] D. Matras, J. Villermaux, *Chem. Eng. Sci.* **1973,** 28, 129-137.

[5] M. de Joannon, A. Cavaliere, T. Faravelli, E. Ranzi, P. Sabia, A. Tregrossi, *Proc. Combust. Inst.* **2005**, 30, 2605-2612.

[6] Y. Y. Li, L. D. Zhang, Z. Y. Tian, T. Yuan, B. Yang, J. Z. Yang, F. Qi, *Energy & Fuels* **2009**, *23*, 1473-1485.

[7] Kamphus, M., Liu, N. N., Atakan, B., Qi, F., McIlroy, A. REMPI temperature measurement in molecular beam sampled low-pressure flames. *Proc. Combust. Inst.* **2002**, *29*, 2627-2633.

[8] Qi, F., McIlroy, A. Identifying combustion intermediates via tunable vacuum ultraviolet photoionization mass spectrometry. *Combust. Sci. Technol.* **2005**, *177*, 2021-2037.

[9] Linstrom, P. J., Mallard, W. G., *NIST Chemistry Webbook*, National Institute of Standard and Technology, Number 69, Gaithersburg, MD, 2008, http://webbook.nist.gov.
[10] R.J. Kee, F.M. Rupley, J.A. Miller, *Chemkin II: A fortran chemical kinetics package for the analysis of a gas-phase chemical kinetics*, SAND89-8009B, Sandia Laboratories, **1993**.
[11] F. Buda, R. Bounaceur, V. Warth P.A. Glaude, R. Fournet, F. Battin-Leclerc, *Combust. Flame* **2005**, 142, 170-186.
[12] V. Warth, N. Stef, P.A. Glaude, F. Battin-Leclerc, G. Scacchi, G.M. Côme, *Combust. Flame* **1998**, 114, 81-102.
[13] S. Touchard, R. Fournet, P.A. Glaude, V. Warth, F. Battin-Leclerc, G. Vanhove, M. Ribaucour, R. Minetti., *Proc. Combust. Inst.* **2005**, 30, 1073-1081.
[14] C. Muller, V. Michel, G. Scacchi, G.M. Côme, *J. Chim. Phys.* **1995**, 92, 1154-1178.
[15] S.W. Benson, *Thermochemical Kinetics*, 2nd ed., John Wiley, New York, **1976**.